Parametric studies on convection during the physical vapor transport of mercurous chloride (Hg₂Cl₂)

Geug-Tae Kim[†] and Kyong-Hwan Lee*

Department of Nano-Bio Chemical Engineering, Hannam University, Taejon 306-791, Korea
Clean Energy Research Department, Korea Institute of Energy Research, Taejon 305-343, Korea

Abstract The temperature hump is found to be most efficient in suppressing parasitic nucleation. With the temperature humps, there are found to be observed in undersaturations along the transport path for convective-diffusive processes ranging from $D_{AB} = 0.0584$ cm²/s to 0.584 cm²/s, axial positions from 0 to 7.5 cm. With decreasing Ar = 5 to 3.5, the temperature difference is increased because of the imposed nonlinear temperature profile but the rate is decreased. For $2 \leq$ Ar ≤ 3.5, the rate is increased with the aspect ratio as well as the temperature difference. Such an occurrence of a critical aspect ratio is likely to be due to the effect of sidewall and much small temperature difference. The rate is decreased exponentially with the aspect ratio for $2 \leq$ Ar ≤ 10. Also, the rate is exponentially decreased with partial pressure of component B, P_B for $1 \leq P_B \leq 100$ Torr.

Key words Mercurous chloride, Convection, Physical vapor transport

1. Introduction

Interest in growing mercurous chloride (Hg₂Cl₂) single crystal stems from their exceptional optical broad transmission range from 0.36 to 20 μm for applications in acousto-optic and opto-electronic devices such as Bragg cells, X-ray detectors operating at ambient temperature [1]. The equimolar Hg₂Cl₂ compound decomposes to two liquids at a temperature near 525°C where the vapor pressure is well above 20 atm [2, 3]. Because of this decomposition and high vapor pressure, Hg₂Cl₂ cannot be solidified as a single crystal directly from the stoichiometric melt. However, very similar to the mercurous bromide, mercurous chloride exhibits sufficiently high vapor pressure at low temperatures so that these crystals are usually grown by the physical vapor transport (PVT) in closed silica glass ampoules. The PVT processing has many advantages over melt-growth methods since it can be conducted at low temperatures: (1) vapor-solid interfaces possess relatively high interfacial morphological stability against non-uniformities in heat and mass transfer; (2) high purity crystals are achieved; (3) materials decomposed before melting, such as Hg₂Cl₂ can be grown; (4) lower point defect and dislocation densities are achieved [4]. The mechanism of the PVT process is simple: sublimation-condensation in closed silica glass ampoules in temperature gradient imposed between the source material and the growing crystal. In the PVT system of Hg₂Cl₂, the molecular species Hg₂Cl₂ sublimes as the vapor phase from the crystalline source material (Hg₂Cl₂), and is subsequently transported and re-incorporated into the single crystalline phase (Hg₂Cl₂) [5]. Recently PVT has become an important crystal growth process for a variety of acousto-optic materials. However, the industrial applications of the PVT process remain limited. One of important main reasons is that transport phenomena occurring in the vapor are complex and coupled so that it is difficult to design or control the process accurately. Such complexity and coupling are associated with the inevitable occurrence of thermal and/or solutal convection generated by the interaction of gravity with density gradients arising from temperature and/or concentration gradients. In general, convection has been regarded as detrimental and, thus, to be avoided or minimized in PVT growth system. These thermal and/or solutal convection-induced complications result in problems ranging from crystal inhomogeneity to structural imperfection. Therefore, in order to analyze and control the PVT process accurately, and also make significant improvements in the process, it is essential to investigate the roles of convection in the PVT process.

Markham, Greenwell and Rosenberger [6] examined the effects of thermal and thermosolutal convections during the PVT process inside vertical cylindrical enclosures for a time-independent system, and showed that even in the absence of gravity, convection can be present, caus-

[†]Corresponding author
Tel: +82-42-629-7984
Fax: +82-42-623-9489
E-mail: gtkim@hannam.ac.kr

ing nonuniform concentration gradients. They emphasized the role of geometry in the analysis of the effects of convection. As such these fundamentally constitute steady state two-dimensional models. The steady state models are limited to low Rayleigh number applications, because as the Rayleigh number increases oscillation of the flow field occurs. To address the issue of unsteady flows in PVT, Duval [7] performed a numerical study on transient thermal convection in the PVT processing of Hg_2Cl_2 very similar to the mercurous bromide for a vertical rectangular enclosure with insulated temperature boundary conditions for Rayleigh numbers up to 10^6. Nadarajah et al. [8] addressed the effects of solutal convection for any significant disparity in the molecular weights of the crystal components and the inert gas. Zhou et al. [9] reported that the traditional approach of calculating the mass flux assuming one-dimensional flow for low vapor pressure systems is indeed correct. Rosenberger et al. [10] studied three-dimensional numerical modeling of the PVT yielded quantitative agreement with measured transport rates of iodine through octofluorocyclobutane (C_4F_8) as inert background gas in horizontal cylindrical ampoules.

In this theoretical study, a two-dimensional model is used for the analysis of the PVT processes during vapor-growth of mercurous chloride (Hg_2Cl_2) crystals in horizontally oriented, cylindrical, closed ampoules in a two-zone furnace system. Diffusion-limited processes are considered in this paper, although the recent paper of Singh, Mazelsky and Glicksman [11] demonstrated that the interface kinetics plays an important role in the PVT system of Hg_2Cl_2. Thermo-solutal convection will be considered at this point, primarily because a mixture of Hg_2Cl_2 vapor and impurity of argon (Ar). Thermal convection can be ignored in comparison to solutally-induced convection for imposed nonlinear thermal profile to prevent supersaturation along the transport path.

It is the purpose of this paper (1) to relate applied convective process parameters such as gravitational acceleration perturbations, molecular weight of an inert gas and partial pressure of an inert gas on the crystal growth and its distributions across an interface (2) to examine the effects of solutal convection with a nonlinear temperature profile in order to gain insights into the underlying physicochemical processes.

2. Physical and Mathematical Formulations

Consider a rectangular enclosure of height H and

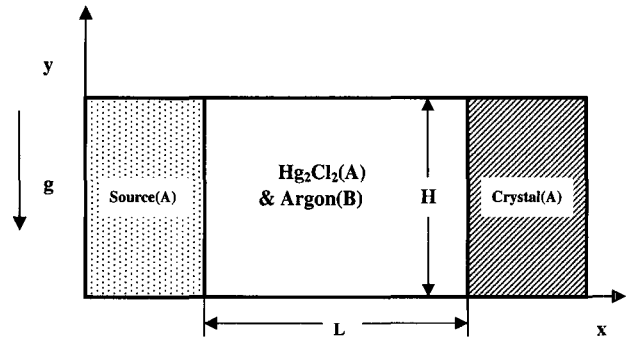

Fig. 1. Schematic of PVT growth reactor in a two-dimensional rectangular system.

transport length L, shown in Fig. 1. The source is maintained at a temperature T_s, while the growing crystal is at a temperature T_c, with $T_s > T_c$. PVT of the transported component A (Hg_2Cl_2) occurs inevitably, due to presence of impurities, with the presence of an inert component B (Ar). The interfaces are assumed to be flat for simplicity. The finite normal velocities at the interfaces can be expressed by Stefan flow deduced from the one-dimensional diffusion-limited model [12], which would provide the coupling between the fluid dynamics and species calculations. On the other hand, the tangential component of the mass average velocity of the vapor at the interfaces vanishes. Thermodynamic equilibria are assumed at the interfaces so that the mass fractions at the interfaces are kept constant at $\omega_{A,s}$ and $\omega_{A,c}$. On the vertical non-reacting walls appropriate velocity boundary conditions are no-slip, the normal concentration gradients are zero, and wall temperatures are imposed as nonlinear temperature gradients.

Thermophysical properties of the fluid are assumed to be constant, except for the density. When the Boussinesq approximation is invoked, density is assumed constant except the buoyancy body force term. The density is assumed to be a function of both temperature and concentration. The ideal gas law and Dalton's law of partial pressures are used. Viscous energy dissipation and the Soret-Dufour (thermo-diffusion) effects can be neglected, as their contributions remain relatively insignificant for the conditions encountered in our PVT crystal growth processes. Radiative heat transfer can be neglected under our conditions, based on Kassemi and Duval [13].

The transport of fluid within a rectangular PVT crystal growth reactor is governed by a system of elliptic, coupled conservation equations for mass (continuity), momentum, energy and species (diffusion) with their appropriate boundary conditions. Let v_x, v_y denote the

velocity components along the x- and y-coordinates in the x, y rectangular coordinate, and let T, ω_A, p denote the temperature, mass fraction of species A (Hg$_2$Cl$_2$) and pressure, respectively.

The dimensionless variables are scaled as follows:

$$x^* = \frac{x}{H}, y^* = \frac{y}{H},$$ (1)

$$u = \frac{u_x}{U_c}, v = \frac{v_y}{U_c}, p = \frac{p}{\rho_c U_c^2},$$ (2)

$$T^* = \frac{T-T_c}{T_s-T_c}, \omega_A^* = \frac{\omega_A-\omega_{A,c}}{\omega_{A,s}-\omega_{A,c}}.$$ (3)

$$\nabla^* \bullet V^* = 0,$$ (4)

$$\vec{V}^* \bullet \nabla^* \vec{V}^* = -\nabla^* p^* + Pr\nabla^{*2}\vec{V}^* - Ra \cdot Pr \cdot T^* \cdot e_g,$$ (5)

$$\vec{V}^* \bullet \nabla^* T^* = \nabla^{*2} T^*$$ (6)

$$\vec{V}^* \bullet \nabla^* \omega_A^* = \frac{1}{Le}\nabla^{*2}\omega_A^*$$ (7)

The dimensionless governing equations are given by:

These nonlinear, coupled sets of equations are numerically integrated with the following boundary conditions:

On the walls ($0 < x^* < L/H$, $y^* = 0$ and 1):

$$u(x^*,0) = u(x^*,1) = v(x^*,0) = v(x^*,1) = 0$$ (8)

$$\frac{\partial\omega_A^*(x^*,0)}{\partial y^*} = \frac{\partial\omega_A^*(x^*,1)}{\partial y^*} = 0,$$

$$T^*(x^*,0) = T^*(x^*,1) = \frac{T-T_c}{T_s-T_c}$$

On the source ($x^* = 0$, $0 < y^* < 1$):

$$u(0,y^*) = -\frac{1}{Le(1-\omega_{A,s})}\frac{\Delta\omega}{\partial x^*}\frac{\partial\omega_A^*(0,y^*)}{\partial x^*},$$ (9)

$$v(0,y^*) = 0,$$
$$T^*(0,y^*) = 1,$$
$$\omega_A^*(0,y^*) = 1.$$

On the crystal ($x^* = L/H$, $0 < y^* < 1$):

$$u(L/H,y^*) = -\frac{1}{Le(1-\omega_{A,c})}\frac{\Delta\omega}{\partial x^*}\frac{\partial\omega_A^*(L/H,y^*)}{\partial x^*}$$ (10)

$$v(L/H,y^*) = 0,$$
$$T^*(L/H,y^*) = 0,$$
$$\omega_A^*(L/H,y^*) = 0.$$

The following temperature profile was used as a boundary condition along the ampoule ($y = 0$ and $y = H$): this equation is expressed in reference to an approximate fit of experimental data [14, 15], see Fig. 2.
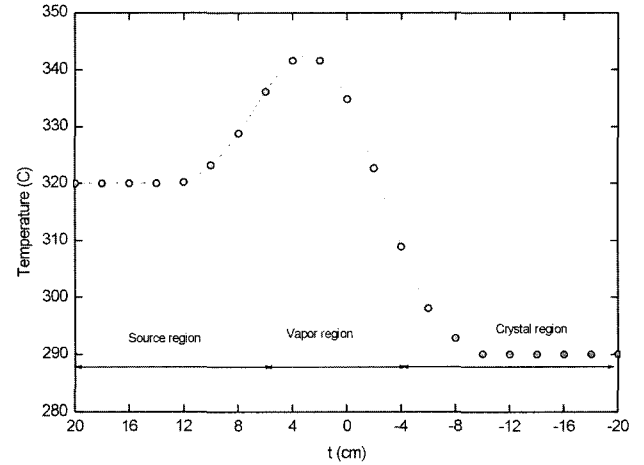

Fig. 2. The temperature profile along the ampoule [14].

$$T(t) = \begin{cases} 563.16 & \text{for } -20 \le t \le -10 \text{ cm} \\ 608 + 4.97t - 0.70t^2 & \text{for } -10 \le t \le -12 \text{ cm} \\ -5.91 \times 10^{-2}t^3 \\ + 6.67 \times 10^{-3}t^4 \\ + 2.60 \times 10^{-4}t^5 \\ -2.49 \times 10^{-5}t^6 \\ 593.16 & \text{for } 12 \le t \le -20 \text{ cm} \end{cases}$$ (11)

Relative to Fig. 2, during the crystal growth the ampoule is placed in the nonlinear thermal profile as shown in Fig. 3. The hump region corresponds to the location of the vapor component A and B inside the ampoule. The source material lies in the region with the larger temper-
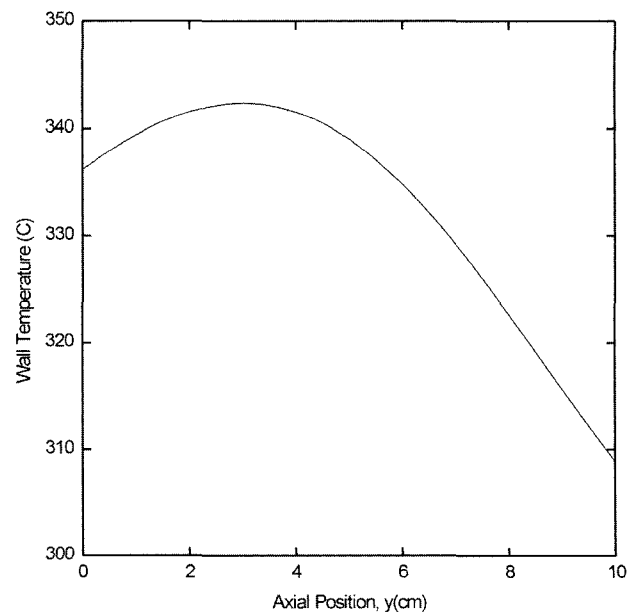

Fig. 3. An axial temperature profile given by Eq. (11) with maximum ("hump") between T_s and T_c.

ature near $t \geq 8$ cm. Whereas crystal growth occurs in the region corresponding to $t \leq -4$ cm. In our experiments one positions the ampoule in the growth region with a temperature less than the source in order to drive the process. In addition, the length of the hump region can also be adjusted so that we have a much larger source region. With respect to Fig. 3, the following transformation is used to relate the laboratory reference to the ampoule: where K_i is

$$x = K_i - t$$

the position of the source and vapor interface in the laboratory reference frame.

In the dimensionless parameters in the governing equations the thermophysical properties of the gas mixture are estimated from gas kinetic theory using Chapman-Enskog's formulas [16].

The vapor pressure [17] p_A of Hg_2Cl_2 (in the unit of Pascal) can be evaluated from the

$$p_A = e^{(a - b/T)}, \tag{12}$$

following formula as a function of temperature: in which $a = 29.75$, $b = 11767.1$.

The crystal growth rate V_c could be found in Ref. [9]. The detailed numerical schemes in order to solve the discretization equations for the system of nonlinear, coupled governing partial differential equations are found in Ref. [18].

3. Results and Discussion

The parametric study is useful for showing trends and generalizing the problem, but many parameters are involved in the problem under consideration, which renders it difficult for a general analysis. One of the purposes for this study is to correlate the growth rate and the interfacial distributions, and partial pressure of A (p_A) to process parameters such as molecular weight of B (M_B), gravity level, nonlinear and linear thermal profile, and binary diffusivity for a particular material (Hg_2Cl_2). Thus, it is desirable to express some results in terms of dimensional growth rate, however they are also applicable to parameter ranges over which the process varies in the manner given. The six dimensionless parameters, namely Gr, Ar, Pr, Le, C_v and Pe, are independent and arise naturally from the dimensionless governing equations and boundary conditions. The dimensionless parameters and physical properties for the operating conditions of this study are shown in Table 1.

Table 1
Typical thermo-physical properties used in this study ($M_A = 472.086$, $M_B = 39.95$)

Transport length, L	10 cm
Height, H	2 cm
Source temperature, T_s	336.21
Crystal temperature, T_c	308.89
Density, ρ	0.002048 g/cm^3
Dynamic viscosity, μ	0.00029 g/(cm•sec)
Diffusivity, D_{AB}	0.584 cm^2/s
Thermal expansion coefficient, β	0.0017 K^{-1}
Prandtl number, Pr	0.667
Lewis number, Le	0.47
Peclet, Pe	3.57
Concentration number, Cv	1.029
Total system pressure, P_T	266.36 Torr
Thermal grashof number, Gr_t	1.05×10^4
Solutal grashof number, Gr_s	1.72×10^5

In this study, the effects of an inert component whose molecular weight is not equal to that of the crystal component during the physical vapor transport. In this case $M_A \neq M_B$; both solutal and thermal effects are considered. If solutal convection is dominant, the imposed temperature profile has little effect on the growth rate [8]. Conductive wall boundary conditions with a nonlinear thermal profile are considered, while the insulated walls are not considered because it is difficult to obtain in practice and most of vapor growth experiments are performed under the imposed nonlinear thermal profile to avoid nucleation at the ampoule walls. Figure 3 shows the axial temperature profile given by Eq. (11) with maximum ("hump") between T_s and T_c. To prevent undesirable nucleations at the walls, an often used experimental technique is to impose a nonlinear thermal profile with a maximum between the crystal and the source, and is usually referred to as a temperature "hump". This temperature hump could eliminate the problem of vapor supersaturation along the transport path and, thus, of parasitic nucleations at the walls. But, these humps may result in sharp temperature gradients near the crystal region, inducing thermal stresses and a decrease in crystal quality. A temperature hump of 27 K with $T_s = 336$, $T_c = 309$ is selected for this study.

In Fig. 4 the equilibrium vapor transport pressure profile is obtained from Eq. (12) for the hump thermal profile as shown in Fig. 3. The partial pressures of component A (Hg_2Cl_2) at the walls are gained from convective-diffusive transport at the horizontal orientation with $1g_0$ and Ar (aspect ratio: transport length-to-width) of 5. It is clear that the hump thermal profile is necessary for the prevention of nucleation at the walls and the elimi-
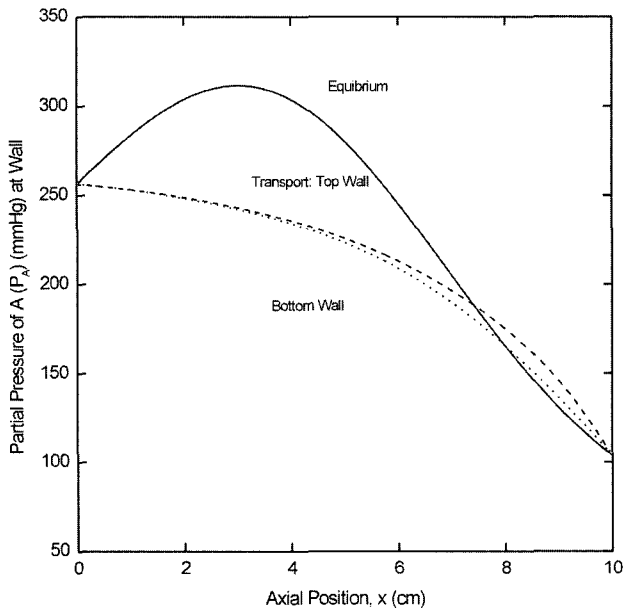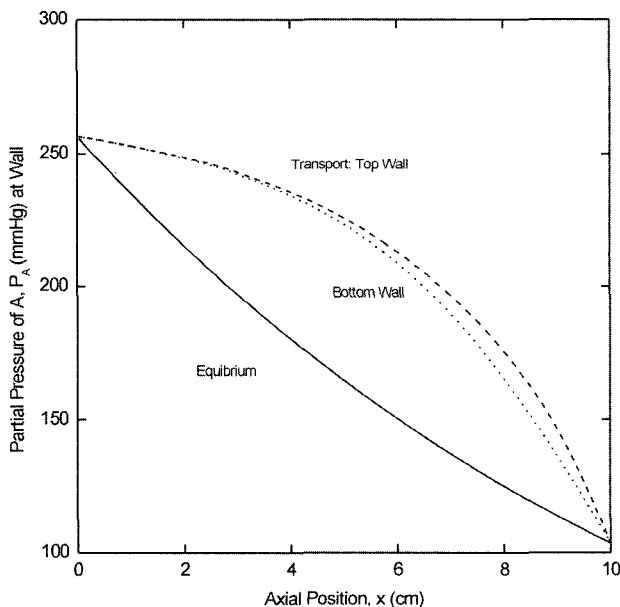
Fig. 4. An axial distribution of partial pressures of component A at the walls resulting from diffusive-convective transport at $g_y = 1g_0$, and equilibrium vapor transport pressure, for Ar (L/H) = 5 and the nonlinear wall temperature profile of Fig. 3.

nation of supersaturation along the transport path. For $7.5 \leq x \leq 10$ cm, the supersaturation of vapor A (Hg_2Cl_2) occurs due to wall temperatures lower than temperatures at top and bottom walls inside an ampoule, which is directly related to the convective-diffusive flow pattern [8, 19], not shown here. Therefore, to avoid the par-

asitic nucleation of the component A near the crystal region, a larger hump profile near the crystal would be necessary, which is realistic in experiments. The higher concentration along the top wall reflects the clockwise sense of rotation of the solutal convection.

Figure 5 shows that with a linear temperature profile, the vapor of component A (Hg_2Cl_2) is in a supersaturation throughout the ampoule. It is clear to see why a linear temperature profile is rarely used in practice. Figure 6 shows that axial distribution of partial pressures of component A for a system with the same conditions as for Fig. 4 with $D_{AB} = 0.584$ cm^2/s, except for a binary diffusion coefficient of 0.0584 cm^2/s. The much small value of the diffusion coefficient can be obtained when inert gases of larger molecular weight or hydrogen pairs at higher total pressure. In this study, instead of using either inert gases with larger molecule weight or the hydrogen pairs, the diffusion coefficient of 0.584 cm^2/s in Fig. 4 is intentionally decreased by a factor of an one-tenth and reduced to 0.0584 cm^2/s in Fig. 6 for the study of the effects of diffusion transport on axial distribution of partial pressures of component A (Hg_2Cl_2). As shown in Fig. 6, with lower diffusion coefficients, a convection mode is predominant over a diffusion mode because of more diffusion-limited so that the occurrence of supersaturation near the crystal region would arise, reflecting a relatively small hump profile of partial pressure of A. Figure 6 shows a remarkable difference in partial pressure of A between top and bottom
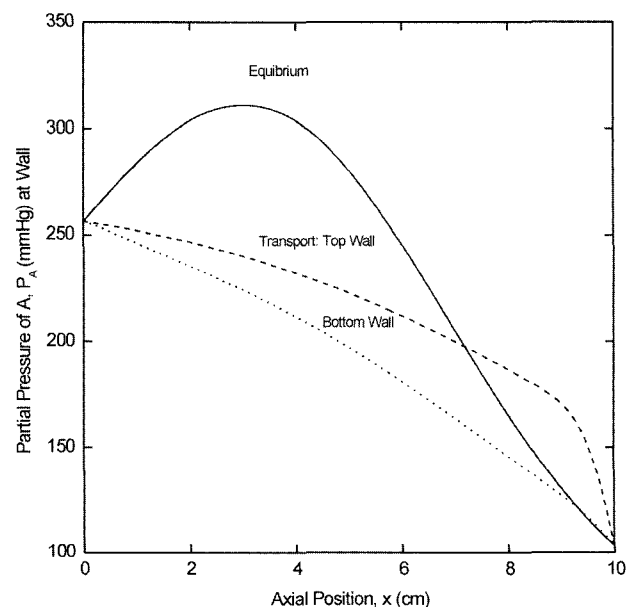

Fig. 5. An axial distribution of partial pressures of component A at the walls resulting from diffusive-convective transport at $g_y = 1g_0$, and equilibrium vapor transport pressures, for Ar (L/H) = 5 and the linear wall temperature profile.

Fig. 6. An axial distribution of partial pressures of component A (Hg_2Cl_2) for system as in Fig. 4 except for $D_{AB} = 0.0584$ cm^2/s.
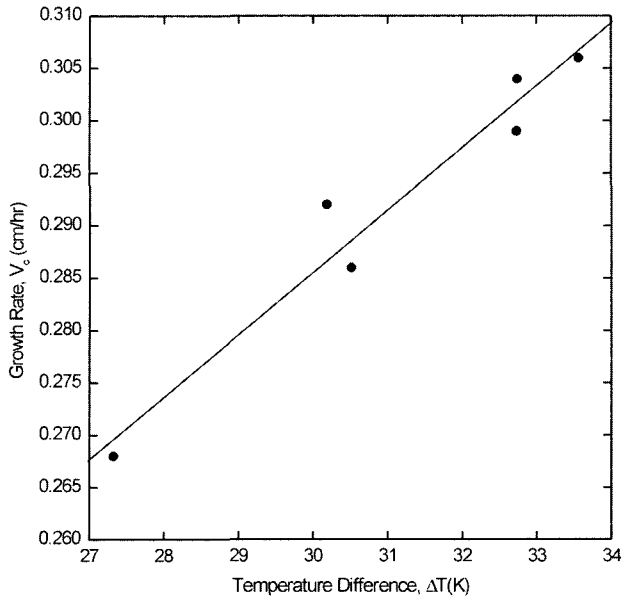
Fig. 7. The effects of the temperature difference between the source and the crystal on the crystal growth rates of Hg_2Cl_2 for the nonlinear conducting walls.
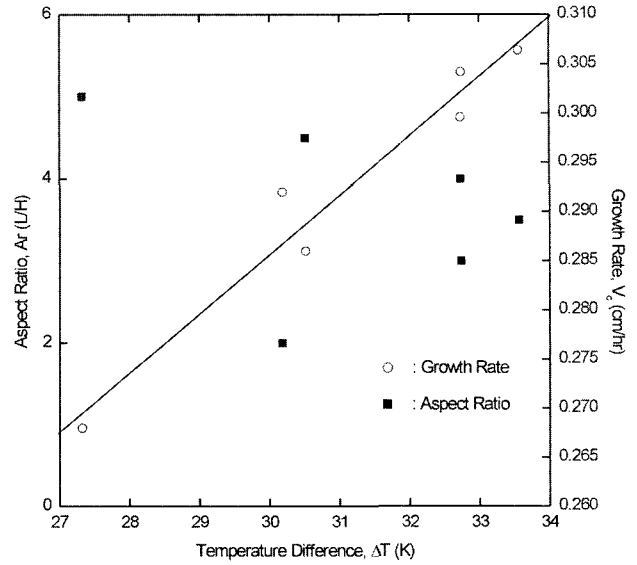

Fig. 8. The effects of both the aspect ratio and the temperature difference on the crystal growth rates of of Hg_2Cl_2 for the nonlinear conducting walls, corresponding to Fig. 7. The symbols of ■ and ○ mean the aspect ratio and the growth rate, respectively.

walls in a comparison with Fig. 4. It is due to the effects of diffusion-limited convection near the crystal region. As discussed later, under lower gravity environments, the diffusion is dominated so that a smaller hump thermal profile would be quite appropriate for suppressing the parasitic nucleation near the crystal. The temperature dependence of the diffusivity on the nonlinear thermal profile is reflected through a binary diffusion coefficient as a function of temperature, which can be calculated from Chapman-Enskog's formula [16]. But, the effect of nonlinear temperature humps would be negligible because of small temperature difference employed.

Figure 7 shows the effects of the temperature difference between the source and the crystal on the crystal growth rates of Hg_2Cl_2 for the nonlinear conducting walls. The aspect ratios under considerations range from 2 up to 5 so that the transport lengths would be limited due to the fixed nonlinear wall thermal profile as shown in Fig. 2. The resulting temperature differences are ranged from 27 through 34 K. As seen in Fig. 7, the rate is directly related and linearly proportional to the temperature difference for $27 \leq \Delta T \leq 34$ K. As shown in Fig. 8, the relationship between the aspect ratio, Ar (L/H) and the temperature difference, ΔT (K) proves to be similar to the nonlinear temperature profile of Fig. 2, which is not surprised to get such a result. The symbols of ■ and ○ mean the aspect ratio and the growth rate, respectively. Figure 8 clearly explains the reason why the rate is decreased with increasing ΔT from 27 to

34 K. In other words, when the aspect ratio is increased, the growth rate increases. As discussed in details later, the aspect ratio is based on the fixed width of 2 cm so that the transport length L is varied from 4 to 10 cm which corresponds from Ar = 2 to 5. The critical aspect ratio is 3.5. With decreasing Ar = 5 to 3.5, the temperature difference is increased because of the imposed nonlinear temperature profile but the rate is decreased. For
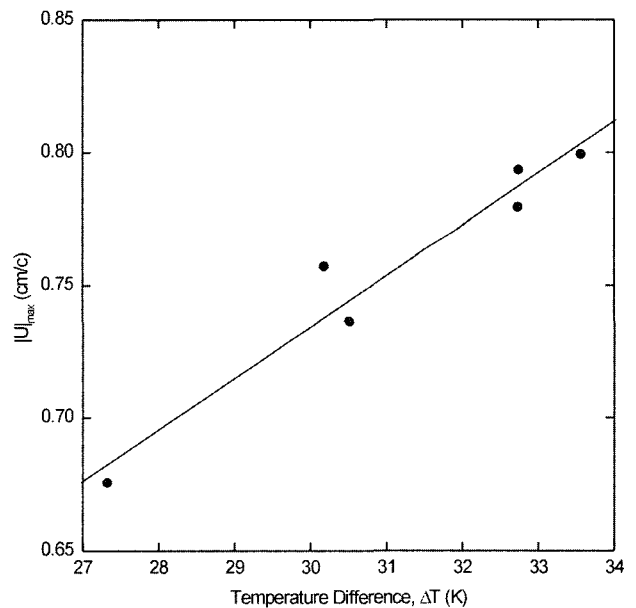

Fig. 9. The effects of the temperature difference between the source and the crystal on the maximum velocity magnitude, $|U|_{max}$, for the nonlinear conducting wall, corresponding to Fig. 7.

$2 \le Ar \le 3.5$, the rate is increased with the aspect ratio as well as the temperature difference. Such an occurrence of a critical aspect ratio is likely to be due to the effect of sidewall and much small temperature difference. This result is consistent with Singh *et al.'* results [22]. Figure 9 shows the effects of the temperature difference between the source and the crystal on the maximum velocity magnitude, $|U|_{max}$, for the nonlinear conducting wall, corresponding to Fig. 7. The maximum velocity magnitude, $|U|_{max}$ plays a role of gauge which represents an intensity of convection. Figure 7 has the slope of 0.00615 cm/hr/K, while Fig. 9 has that of 0.01982 cm/s/K. But it is hard to compare Fig. 7 with Fig. 9 from a viewpoint of quantity, it is inferred that the rates of Hg$_2$Cl$_2$ are significantly governed by thermo-solutal convection. Note that convection is caused by either temperature or solutal gradients in a system under consideration so that it is referred as thermo-solutal convection.

Figure 10 shows the effect of aspect ratio, Ar (L/H) on the crystal growth rates of Hg$_2$Cl$_2$. For the study of the effect of aspect ratio, the transport length L is invariant and the width H is varied from 1 to 5 so that the aspect ratio Ar ranges from 10 down to 2. The rate is decreased exponentially with the aspect ratio. In other words, the rate is sharply decreased from 2 to 5, and then slowly decreased for $5 \le Ar \le 10$. It is likely to be due to the effect of sidewall. Figure 11 shows the effect of aspect ratio on the maximum velocity magnitude,
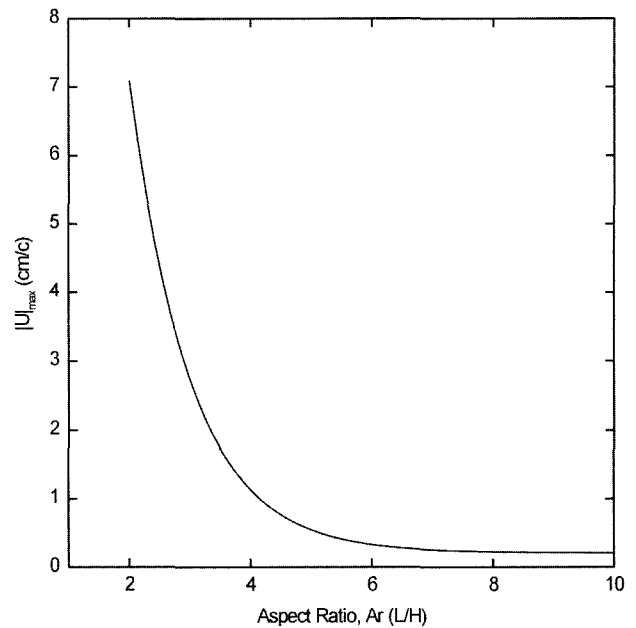

Fig. 11. The influence of aspect ratio, Ar (L/H) on the maximum velocity magnitude, $|U|_{max}$, corresponding to Fig. 10.

$|U|_{max}$ corresponding to Fig. 10. It should be emphasized again that in Fig. 8 the transport length L is varied from 5 to 10, with a width of 2 cm fixed, and the corresponding aspect ratio ranges from 2 to 5. Figure 12 shows the effect of partial pressure of component B, PB (Torr) on the crystal growth rates of Hg$_2$Cl$_2$. The effect of partial pressure of component B, P$_B$ (Torr) is in the main reflected through the binary diffusion coefficient.
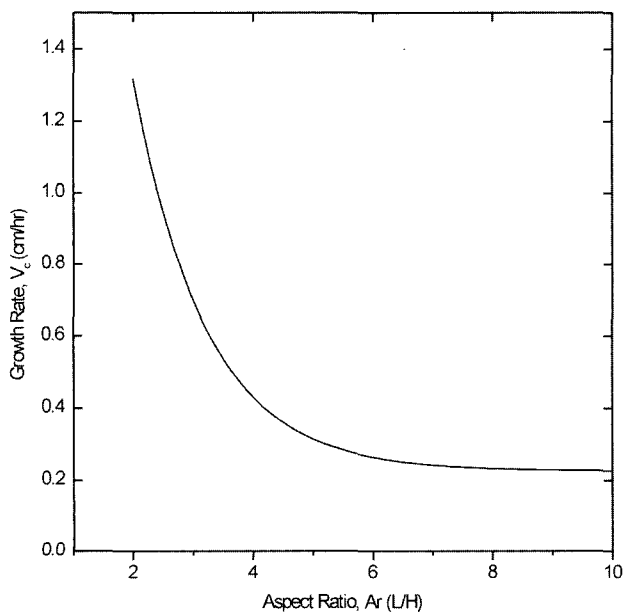

Fig. 10. The influence of aspect ratio, Ar (L/H) on the crystal growth rates of Hg$_2$Cl$_2$.
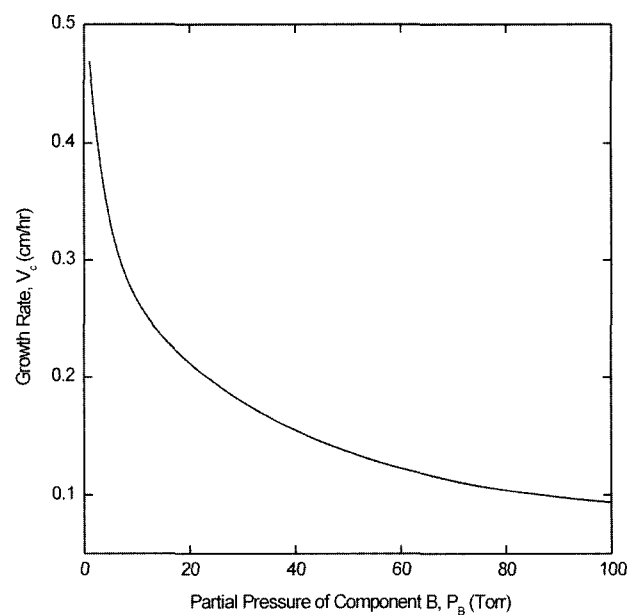

Fig. 12. The effect of partial pressure of component B, P$_B$ (Torr) on the crystal growth rates of Hg$_2$Cl$_2$.
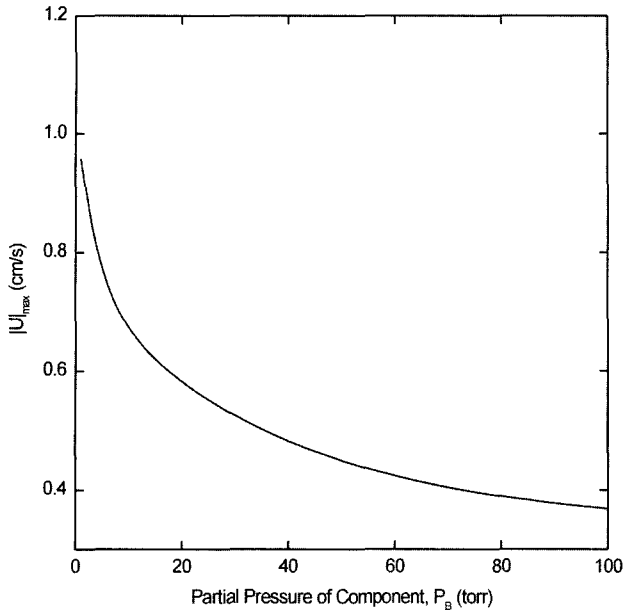
Fig. 13. The effect of partial pressure of component B, P_B (Torr) on the maximum velocity magnitude, $|U|_{max}$, corresponding to Fig. 12.

Like the aspect ratio, the rate is exponentially decreased with partial pressure of component B, P_B. As the partial pressure of B is increased, the binary diffusion coefficient is decreased so that mass transfer by diffusion would be reduced. Figure 13 shows the effect of the partial pressure of B on the maximum velocity magnitude, $|U|_{max}$ corresponding to Fig. 12. Figure 14 shows
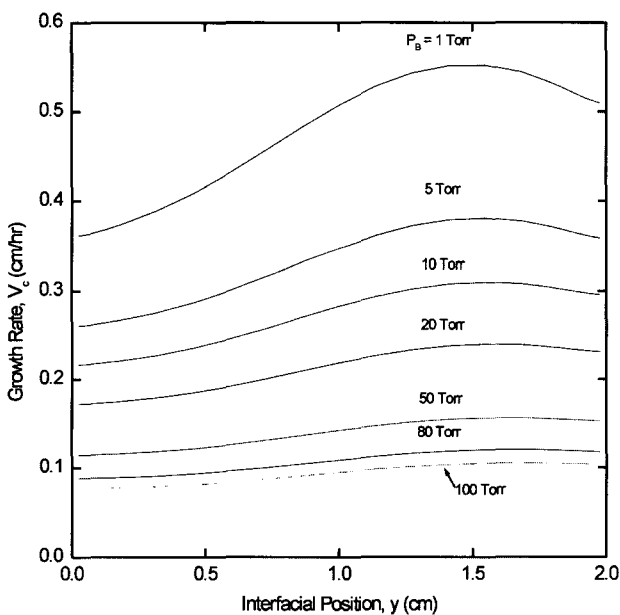

Fig. 14. Interfacial distribution of the crystal growth rates of Hg_2Cl_2 for the various partial pressures of component B, P_B (Torr).

the interfacial distribution of the crystal growth rates of Hg_2Cl_2 for $1 \leq P_B \leq 100$ Torr.

4. Conclusions

For the case when the solutally driven convection ($Gr_s = 1.72 \times 10^5$) due to the disparity in the molecular weights of the component A (Hg_2Cl_2) and B (Ar) is stronger than thermally driven convection ($Gr_t = 1.05 \times 10^4$) with an aspect ratio of 5, total pressure of 266 Torr, Pr = 0.667, Le = 0.47, Pe = 3.57, $C_v = 1.029$, parametric studies on convection during the physical vapor transport of Hg_2Cl_2 are investigated. The temperature hump is found to be most efficient in suppressing parasitic nucleation. With the temperature humps, there are found to be observed in undersaturations along the transport path for convective-diffusive processes ranging from $D_{AB} = 0.0584$ cm^2/s to 0.584 cm^2/s, axial positions from 0 to 7.5 cm. With decreasing Ar = 5 to 3.5, the temperature difference is increased because of the imposed nonlinear temperature profile but the rate is decreased. For $2 \leq Ar \leq$ 3.5, the rate is increased with the aspect ratio as well as the temperature difference. Such an occurrence of a critical aspect ratio is likely to be due to the effect of sidewall and much small temperature difference. This result is consistent with Singh *et al.'* results [22]. Furthermore researches on this result would be performed in the nearest future publications. The rate is decreased exponentially with the aspect ratio for $2 \leq Ar \leq 10$. Also, the rate is exponentially decreased with partial pressure of component B, P_B for $1 \leq P_B \leq 100$ Torr.

References

[1] N. B. Singh, M. Gottlieb, G.B. Brandt, A.M. Stewart, R. Mazelsky and M.E. Glicksman, "Growth and characterization of mercurous halide crystals:mercurous bromide system", J. Crystal Growth 137 (1994) 155.

[2] N.B. Singh, R.H. Hopkins, R. Mazelsky and J.J. Conroy, "Purification and growth of mercurous chloride single crystals", J. Crystal Growth 75 (1970) 173.

[3] S.J. Yosim and S.W. Mayer, "The mercury-mercuric chloride system", J. Phys. Chem. 60 (1960) 909.

[4] F. Rosenberger, "Fluid dynamics in crystal growth from vapors", Physico-Chemical Hydro-dynamics 1 (1980).

[5] N.B. Singh, M. Gottlieb, A.P. Goutzoulis, R.H. Hopkins and R. Mazelsky, "Mercurous Bromide acousto-optic devices", J. Crystal Growth 89 (1988) 527.

[6] B.L. Markham, D.W. Greenwell and F. Rosenberger, "Numerical modeling of diffusive-convective physical vapor transport in cylindrical vertical ampoules", J.

Crystal Growth 51 (1981) 426.

[7] W.M.B. Duval, "Convection in the physical vapor transport process-- I: Thermal", J. Chemical Vapor Deposition 2 (1994) 188.

[8] A. Nadarajah, F. Rosenberger and J. Alexander, "Effects of buoyancy-driven flow and thermal boundary conditions on physical vapor transport", J. Crystal Growth 118 (1992) 49.

[9] H. Zhou, A. Zebib, S. Trivedi and W.M.B. Duval, "Physical vapor transport of zinc-telluride by dissociative sublimation", J. Crystal Growth 167 (1996) 534.

[10] F. Rosenberger, J. Ouazzani, I. Viohl and N. Buchan, "Physical vapor transport revised", J. Crystal Growth 171 (1997) 270.

[11] N.B. Singh, R. Mazelsky and M.E. Glicksman, "Evaluation of transport conditions during PVT: mercurous chloride system", PhysicoChemical Hydrodynamics 11 (1989) 41.

[12] F. Rosenberger and G. Müller, "Interfacial transport in crystal growth, a parameter comparison of convective effects", J. Crystal Growth 65 (1983) 91.

[13] M. Kassemi and W.M.B. Duval, "Interaction of surface radiation with convection in crystal growth by physical vapor transport", J. Thermophys. Heat Transfer 4 (1989) 454.

[14] N.B. Singh and W.M.B. Duval, "Growth kinetics of physical vapor transport processes: crystal growth of the optoelectronic material mercurous chloride", NASA Technical Memorandum 103788 (1991).

[15] C. Mennetrier, W.M.B. Duval and N.B. Singh, "Physi-cal vapor transport of mercurous chloride under a nonlinear thermal profile", NASA Technical Memorandum 105920 (1992).

[16] R.B. Bird, W.E. Stewart and E.N. Lightfoot, Transport Phenomena (New York, NY: John Wiley and Sons, 1960).

[17] C. Mennetrier and W.M.B. Duval, "Thermal-solutal convection with conduction effects inside a rectangular enclosure", NASA Technical Memorandum 105371 (1991).

[18] S.V. Patankar, Numerical Heat Transfer and Fluid Flow (Washington D.C.: Hemisphere Publishing Corp., 1980).

[19] G.T. Kim, W.M.B. Duval, M.E. Glicksman and N.B. Singh, "Thermal convective effects on physical vapor transport growth of mercurous chloride (Hg_2Cl_2) crystals for axisymmetric 2D cylindrical enclosure", Modelling simu. Mater. Sci. Eng. 3 (1995) 331.

[20] I. Catton, "Effect of wall conducting on the stability of a fluid in a rectangular region heated from below", J. Heat Transfer 94 (1972) 446.

[21] G.T. Kim and M.H. Kwon, "Lead bromide crystal growth from the melt and characterization: the effects of nonlinear thermal boundary conditions on convection during physical vapor crystal growth of mercurous bromide", J. Korean Crystal Growth and Crystal Technology 14 (2004) 160.

[22] N.B. Singh, M. Gottlieb, R.H. Hopkins, R. Mazelsky, W.M.B. Duval and M.E. Glicksman, "Physical vapor transport growth of mercurous chloride crystals", Prog. Crystal Growth and Charact. 27 (1993) 201.